

# MSMDFusion: Fusing LiDAR and Camera at Multiple Scales with Multi-Depth Seeds for 3D Object Detection

Yang Jiao<sup>1,2\*</sup>, Zequn Jie<sup>3\*</sup>, Shaoxiang Chen<sup>3</sup>, Jingjing Chen<sup>1,2</sup>, Xiaolin Wei<sup>3</sup>, Lin Ma<sup>3</sup>, and Yu-Gang Jiang<sup>1,2</sup>

<sup>1</sup>Shanghai Key Lab of Intell. Info. Processing, School of CS, Fudan University

<sup>2</sup>Shanghai Collaborative Innovation Center on Intelligent Visual Computing

<sup>3</sup>Meituan

## Abstract

Fusing LiDAR and camera information is essential for achieving accurate and reliable 3D object detection in autonomous driving systems. However, this is challenging due to the difficulty of combining multi-granularity geometric and semantic features from two drastically different modalities. Recent approaches aim at exploring the semantic densities of camera features through lifting points in 2D camera images (referred to as “seeds”) into 3D space for fusion, and they can be roughly divided into (1) early fusion of raw points that aims at augmenting the 3D point cloud at early input stage, and (2) late fusion of BEV (bird’s-eye view) maps that merges LiDAR and camera BEV features before the detection head. While both have their merits in enhancing the representation power of the combined features, this single-level fusion strategy is a suboptimal solution to the aforementioned challenge. Their major drawbacks are the inability to sufficiently interact the multi-granularity semantic features from two distinct modalities, and the lack of ideal 3D geometric information in lifted 2D points. To this end, we propose a novel framework which focuses on the multi-scale progressive interaction of the multi-granularity LiDAR and camera features. Inside the framework are two important designs. First, a Multi-Depth Unprojection method is used to enhance the depth quality of the seeds lifted from pixel space at each interaction level. Second, a Modality-Specific sparse-convolution (MS-Conv) module is applied to aggregate local information and progressively combine geometric and semantic features into a unified space. Together they provide the detection head with more comprehensive features from LiDAR and camera. Our proposed method, abbreviated as MDMSFusion, achieves state-of-the-art results in 3D object detection, with 69.1 mAP and 71.8 NDS on nuScenes validation set, and 70.8 mAP and 73.2 NDS on nuScenes test set, which rank 1st and 2nd respectively among single-model non-ensemble approaches by the time of the submission. Code will be released at <https://github.com/SxJyJay/MSMDFusion>.

## 1 Introduction

3D object detection (Zhou and Tuzel 2018; Yan, Mao, and Li 2018; Bai et al. 2022), which aims at recognizing and locating a set of categories of objects in the 3D scene, is of vital importance to autonomous driving. In order to improve the robustness of detection results, the LiDAR and the camera, as two sensors which can provide complementary

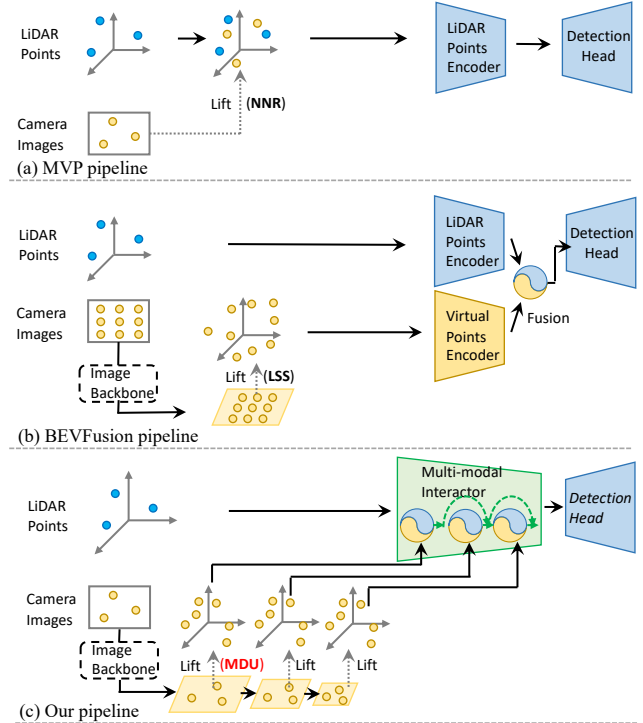


Figure 1: Framework comparison of (a) MVP, (b) BEVFusion, and (c) our MSMDFusion. Our approach differs from them in two major aspects: First, MSMDFusion interacts LiDAR and camera features at multiple stages rather than at a single stage. Second, within each stage, a novel seed lifting strategy, named Multi-Depth Unprojection (MDU), is devised for efficiently generating reliable 3D virtual points. MVP and BEVFusion respectively adopt Nearest Neighbor Retrieval (NNR) and LSS (Phlion and Fidler 2020) as lifting strategy.

signals, are widely equipped on autonomous driving vehicles (e.g., nuScenes (Caesar et al. 2020) self-driving cars have 6 cameras and 1 LiDAR). LiDARs can capture accurate spatial information in the form of 3D point clouds, while cameras capture rich semantics with 2D images. Therefore, developing multi-modal detectors that enjoy the benefits of

\*These authors contributed equally.

the two worlds is promising. Such an idea has catalyzed the emergence of a set of recent researches (Chen et al. 2017b; Liang et al. 2018; Qi et al. 2018; Yoo et al. 2020; Vora et al. 2020; Wang et al. 2021; Yin, Zhou, and Krähenbühl 2021; Bai et al. 2022; Liu et al. 2022; Liang et al. 2022).

A large number of early works (Chen et al. 2017b; Liang et al. 2018, 2019; Sindagi, Zhou, and Tuzel 2019; Yoo et al. 2020; Vora et al. 2020; Wang et al. 2021; Bai et al. 2022) perform LiDAR-camera fusion by projecting the sparse 3D queries onto 2D image planes as the positional prior, then collecting useful 2D semantic features to enrich their 3D counterparts. These 3D queries can be raw points (Liang et al. 2018; Vora et al. 2020; Wang et al. 2021), region proposals (Chen et al. 2017b), or both (Yoo et al. 2020; Bai et al. 2022). However, this line of approaches suffer from the sparsity of LiDAR points. Since LiDAR points are much sparser than camera pixels, such a projection approach will inevitably waste semantically rich 2D features (Bai et al. 2022; Liang et al. 2022).

Recently, another paradigm (Yin, Zhou, and Krähenbühl 2021; Liu et al. 2022; Liang et al. 2022) for LiDAR-camera fusion has emerged. Instead of collecting 2D semantic features with 3D queries, these methods directly lift 2D pixels to the 3D world (we refer to these pixels as “seeds” in this paper), and these lifted points can be treated as 3D points to fuse with the real 3D point cloud at a certain stage of the detection pipeline. MVP (Yin, Zhou, and Krähenbühl 2021) and BEVFusion (Liu et al. 2022) are two representative methods. As shown in Fig.1(a) and (b), MVP carefully selects a set of seeds from each instance in 2D images, and assigns a depth to each seed using a real depth from its nearest neighbor’s 3D counterpart. Then, these seeds, together with semantic labels, are lifted as 3D virtual points to augment the original 3D point cloud as input to an ordinary 3D object detector. In contrast to MVP’s early raw-point fusion strategy, BEVFusion treats every image feature pixel as a seed, and lifts them to the bird’s-eye view (BEV) space with an off-the-shelf depth estimator LSS (Phlion and Fidler 2020) in a learnable fashion, then these lifted points are processed by a separate 3D encoder to produce a BEV map, the LiDAR-camera fusion happens at the BEV level by merging the two BEV maps from both modalities.

Despite their impressive improvements, both MVP and BEVFusion suffer from two major problems. First, their LiDAR-camera fusion happens only at a single level, i.e., fusing either the raw points (MVP) or the BEV maps (BEVFusion) as shown in Fig.1(a) and (b), which is not sufficient to comprehensively combine the geometric and semantic features from LiDAR and camera. At the raw point level, the lifted points from raw images carry only limited semantic information, while at the BEV level, the geometric information has been significantly compressed since it no longer preserves 3D structure. Second, the quality of seeds depth estimation is unsatisfactory, leading to distorted 3D virtual points generated. As suggested in BEVDepth (Li et al. 2022), it is challenging for LSS-style detector (Huang et al. 2021) to output depth-aware features accurately, since it lacks explicit depth supervision. MVP can slightly alleviate this problem by retrieving real depths from nearest

neighbors, however, it measures affinities by 2D Euclidean distances, which ignores the fact that proximity in 2D can not be guaranteed in 3D and distant 3D points may fall in a neighborhood in camera images (Wang et al. 2019).

To address the above issues, we propose MSMDFusion, which encourages multi-granularity LiDAR-camera fusion for 3D object detection. As shown in the Fig.1(c), MSMDFusion progressively interacts camera and LiDAR features at multiple stages. To maintain the fine-grained 3D geometric information, each fusion stage happens in the voxel field of a certain spatial resolution (see Fig.2). Meanwhile, within each stage, there are two novel designs for accurate and efficient multi-modal interaction in the voxel field. First, to enhance the quality of generated virtual points, a Multi-Depth Unprojection strategy (MDU) is proposed, which lifts each instance-aware seed with multiple depths through exploring its neighbors. Such a strategy can generate more reliable virtual points, and we will elaborate more on this in Sec.3.3. Second, with the resulting virtual points and original LiDAR points, we fuse them via a proposed Modality-Specific Convolution (MS-Conv) block. Note that MS-Conv blocks operating at different scales can flexibly interact with each other, thus facilitating multi-granularity information aggregation. Finally, these sufficiently interacted multi-modal voxel features are transformed to the BEV space as an enhanced input to a regular BEV encoder and detection head to generate detection outputs. As shown in Table 2, with 100 times fewer generated virtual points than the two BEVFusion methods (Liang et al. 2022; Liu et al. 2022), our MSMDFusion can still achieve state-of-the-art performances.

In summary, our contributions are threefold: (1) We identify problems with current LiDAR-camera fusion methods and propose a novel MSMDFusion approach, which encourages sufficient LiDAR-Camera feature fusion through a multi-scale architecture. (2) Within each scale, we propose a Multi-Depth Unprojection strategy (MDU) to generate more reliable virtual points, as well as a Modality-Specific Convolution block (MS-Conv) to achieve fine-grained multi-modal interaction at the voxel field. (3) Extensive experimental results on the nuScenes dataset prove the effectiveness of our MSMDFusion and its components. We achieve the state-of-the-art performances on the nuScenes detection track, especially on the challenging test set, we achieve 70.8 mAP and 73.2 NDS, which rank 1st and 2nd respectively among single-model non-ensemble<sup>1</sup> approaches by the time of the submission.

## 2 Related Work

Recently, fusing LiDAR and camera signals in 3D detection has attracted increasing interest. Early works (Chen et al. 2017b; Liang et al. 2018; Vora et al. 2020; Yoo et al. 2020; Huang et al. 2020; Wang et al. 2021) project 3D queries to 2D camera images for collecting useful semantics. Under such a paradigm, MV3D (Chen et al. 2017b) and AVOD (Ku et al. 2018) associate 3D proposals with 2D ROI features. While PointPainting (Vora et al. 2020) and PointAugment-

<sup>1</sup>We do not use Test-Time Augmentation (TTA) which is in fact an ensemble technique.

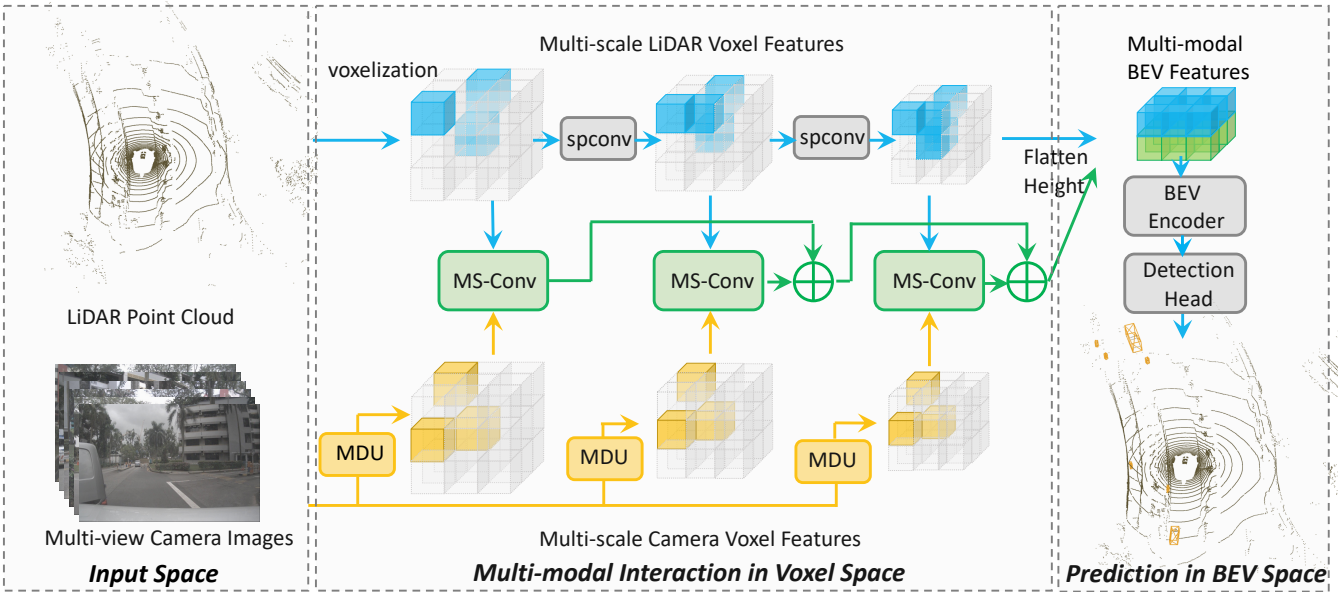


Figure 2: The framework of our proposed MSMDFusion. Given a LiDAR point cloud and corresponding multi-view camera images, MSMDFusion first separately transforms them into the voxel space and obtains multi-scale LiDAR and camera features. Then, the LiDAR and camera features at each scale interact through our proposed Multi-Depth Unprojection strategy (MDU) and Modality-Specific Convolution block (MS-Conv, details in Fig.5). The outputs of MS-Conv at each scale are further aggregated for combining multi-granularity information. Finally, the resulting multi-modal and LiDAR voxel features are flattened into the BEV space for the final prediction.  $\oplus$  represents voxel addition and “spconv” indicates 3D sparse convolution.

ing (Wang et al. 2021) directly decorate raw 3D points with 2D semantics. EP-Net (Huang et al. 2020) and 3DCVF (Yoo et al. 2020) perform multi-modal fusion at both point level and proposal level. However, since 3D points are inherently sparse, such a hard association approach wastes the dense semantic information in 2D features. Toward this end, recent multi-modal 3D detectors (Yin, Zhou, and Krähenbühl 2021; Liang et al. 2022; Liu et al. 2022) lift dense 2D points to 3D space for learning the 2D-3D joint representation in a shared space. MVP (Yin, Zhou, and Krähenbühl 2021) selects pixels from foreground objects and unprojected them to the 3D space for points cloud augmentation. While two BEVFusion methods (Liang et al. 2022; Liu et al. 2022) both densely lift every image pixel into 3D space and then encode these lifted points as another BEV (bird’s-eye view) map to fuse with the BEV map obtained using the original 3D point cloud. LiDAR and camera signals will finally share a common representation space, but they do not interact at any stage before BEV fusion.

### 3 Method

#### 3.1 Framework Overview

In this section, we present the details of our MSMDFusion, as well as the design motivation of the key components in the framework. As shown in Fig.2, given a LiDAR point cloud and corresponding multi-view camera images as inputs, MSMDFusion first extracts multi-scale features from both modalities in the voxel space. Then, within the voxel space, multi-modal progressive interaction is performed at

multiple scales to properly combine multi-granularity information from the two modalities. At each scale, we specifically design a Multi-Depth Unprojection (MDU) strategy to obtain high-quality camera features in the voxel space, and a Modality-Specific Convolution block (MS-Conv) for effective LiDAR-camera interaction and fusion. We also introduce cross-scale connections to progressively combine features of different granularities. Afterward, the deeply interacted multi-modal features, together with the LiDAR features, are transformed into the BEV space and fed to the BEV encoder and detection head for the final prediction. It is worth mentioning that our MSMDFusion is a general framework and the LiDAR branch (blue arrows in Fig.2) can be any voxel-based backbones. Each stage and the corresponding components will be introduced in the following subsections.

#### 3.2 LiDAR and Camera Feature Extraction

We first extract high-level features from the raw inputs of LiDAR and camera. For a given LiDAR point cloud, we voxelize the points and extract their features in the voxel space using a set of 3D sparse convolutional blocks (Graham, Engelcke, and Van Der Maaten 2018) following prior works (Bai et al. 2022; Liu et al. 2022; Liang et al. 2022). Each convolutional block outputs voxel features of different scales, and these multi-scale features will further interact with their 2D counterparts through our proposed MS-Conv blocks.

For the multi-view camera images, we adopt ResNet50 with FPN as the image backbone to extract multi-scale im-

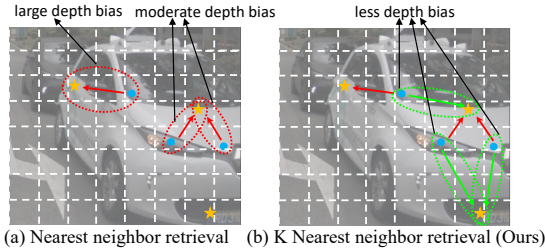


Figure 3: Comparison of the effects of retrieving reference points from nearest neighbor (MVP) and K-nearest neighbor (Ours). The blue circle and yellow star represent seeds and reference points, respectively. To keep the figure concise, we only depict the case that  $K=2$ . Our strategy can obtain more reliable depths by exploring more neighbors.

age features, which contains rich object semantics. However, it is non-trivial to transfer these useful semantics to the 3D voxel field, since images are inherently 2D data. Motivated by recent works (Yin, Zhou, and Krähenbühl 2021; Liu et al. 2022; Liang et al. 2022) which select seeds from the image plane and estimate their depths to lift them as 3D virtual points, we further propose a Multi-Depth Unprojection strategy to lift 2D seeds, which could mitigate a drawback in prior works. The details will be presented in the next subsection.

### 3.3 Multi-Modal Interaction in Voxel Space

The extracted LiDAR and camera features from the previous stage respectively focus on geometric and semantic information, hence the goal of multi-modal interaction is to properly fuse these features into a unified rich representation of the scene. But such interaction in the voxel space faces two key challenges. First, the generated virtual points should reflect accurate geometric structure in the voxel space, otherwise they will distort the real data distribution of the point cloud and lead to degraded performances. Second, the information encapsulated in LiDAR features and camera features is intrinsically different, and they should ultimately be aligned in a joint space. To tackle these challenges, we design a Multi-Depth Unprojection strategy (MDU) to generate more reliable virtual points, as well as a Modality-Specific Convolution block (MS-Conv) to efficiently unify LiDAR and camera features into a joint representation in the voxel space. The MDU and MS-Conv are consistently coupled together within each stage of the multi-scale LiDAR-camera fusion framework as shown in the Fig.2. We will individually introduce the operations of MDU and MS-Conv within a single scale, then on top of them, we describe the complete multi-scale LiDAR-camera interaction process.

**Multi-Depth Unprojection** To lift a 2D camera pixel seed to the 3D space (i.e., the unprojection operation), the depth associated with each seed should be estimated (Wang et al. 2019). We first preliminarily review the unprojection operation of MVP (Yin, Zhou, and Krähenbühl 2021) as shown in Fig.3(a). Formally, given a point cloud  $\mathcal{P}$  =

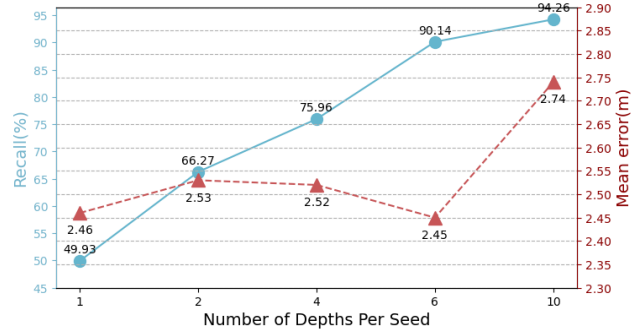


Figure 4: Mean error and recall of the virtual points computed with different number of depths per seed.

$\{(x_i, y_i, z_i)\}_{i=1}^{N_P}$  and multi-view images as inputs, MVP first projects 3D points to 2D space of images and preserve points falling within the 2D foreground instance masks. These 3D points are kept as reference points to provide depth, and they are denoted as  $\mathcal{R} = \{(u_i, v_i, d_i)\}_{i=1}^{N_R}$ , where  $u_i$  and  $v_i$  are pixel coordinates and  $d_i$  is the real depth. Then, a set of seeds  $\mathcal{S} = \{(u_i^s, v_i^s)\}_{i=1}^{N_S}$  are uniformly sampled from each instance mask on the image, and each of them will retrieve a real depth from its nearest reference point as its estimated depth. Finally the sampled seeds with estimated depths can be unprojected to the 3D space as virtual points.

Though effective, MVP ignores the fact that spatial proximity in 2D images can not be guaranteed in 3D, and this may lead to inaccurate depth estimation as shown in the red circle of Fig.3(a). Toward this end, we propose a Multi-Depth Unprojection (MDU) strategy to retrieve K-nearest reference points for each seed, which can be regarded as a soft strategy to achieve more reliable depth estimation. As shown in the green circle of the Fig.3(b), each seed can be unprojected using multiple (K) depths from neighboring reference points, which generates K virtual points to improve its recall of the actual 3D points.

Moreover, we also devise a sampling strategy to efficiently sample seeds from foreground instances in 2D images. Specifically, each instance mask is divided into two regions: boundary and inner region. The inner region is responsible for capturing the surface and the boundary focuses on the contour, and seeds are then uniformly sampled from both regions. The resulting 3D virtual points of unprojection will be voxelized using the same voxel size as the LiDAR voxels in each scale, so as to generate corresponding camera voxel features of the same resolution.

*Discussion on MDU.* Our proposed MDU is a simple yet effective strategy to lift 2D seeds from image to 3D space, and we would like to further discuss one critical problem: will the multiple depths for a seed introduce noise and diminish the benefits? We conducted a quantitative experiment on the nuScenes dataset to investigate this problem. We first preserve a subset  $\mathcal{R}^e = \{(u_i^e, v_i^e, d_i^e)\}_{i=1}^{N^e}$  of the reference points  $\mathcal{R}$ , and use all  $\{(u_i^e, v_i^e)\}$  as seeds to generate virtual points  $\hat{\mathcal{P}}^e$  by retrieving real depths from the remaining reference points  $\mathcal{R} - \mathcal{R}^e$  using MDU. Since the real 3D coordi-

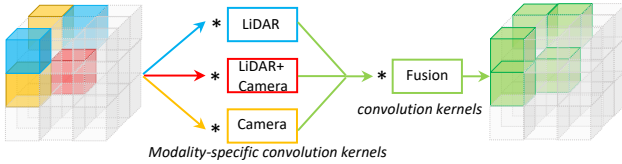


Figure 5: Structure of the Modality-Specific Convolution block (MS-Conv). Arrows and  $*$  represent 3D sparse convolution, and the colors indicate different modalities.

nates  $\mathcal{P}^e$  of the preserved reference points  $\mathcal{R}^e$  are available, we then measure two important metrics for the generated virtual points  $\hat{\mathcal{P}}^e$ : (1) The mean distance error in 3D space between  $\hat{\mathcal{P}}^e$  and  $\mathcal{P}^e$ , which reflects the overall accuracy of the virtual points' coordinates. (2) The recall rate that is the ratio of points in  $\mathcal{P}^e$  which fall within a small neighborhood<sup>2</sup> of at least one point in  $\hat{\mathcal{P}}^e$ , which represents MDU's ability to capture unseen real 3D points. We also vary the number of depths per seed (K) to show its effect. As shown in Fig.4, when the number of K increases from 1 to 6, the recall rate of real points improves dramatically, meanwhile, the mean distance error does not increase significantly. But a too large value of K (e.g., 10) can inevitably introduce noise. This proves that with a properly chosen number of depths, MDU does not lead to increased noise in depth estimation and can generate virtual points with reliable depths while also covering more real points than a single-depth strategy.

**Modality-Specific Convolution** With the resulting LiDAR and camera voxel features that share the same spatial resolution (i.e., the vertically aligned blue and yellow voxels in Fig.2), we aim to learn their joint representations in each scale. This is achieved by the proposed Modality-Specific Convolution (MS-Conv) block as shown in Fig.5. After scattering the LiDAR and camera features into a unified voxel field, non-empty voxels can be divided into three groups according to the modality-wise information they carry: LiDAR-only, camera-only, as well as LiDAR and camera combined, and they are denoted as  $f^L$ ,  $f^C$ , and  $f^{LC}$ , respectively. In order to preserve the modality-specific information of these inputs, our MS-Conv block is also designed to have a set of modality-specific convolution kernels, which will convolve with corresponding inputs:

$$\tilde{f}^m = \Phi(f^m; k^m), \quad (1)$$

where  $m \in \{L, C, LC\}$  represents a specific modality,  $\Phi(\cdot)$  is the 3D sparse convolution operation,  $k^m$  is the modality-specific convolution kernel, and  $\tilde{f}^m$  is the resulting feature. These modality-specific information are now transformed into an intermediate joint space, then within the joint space, we further combine  $\tilde{f}^L$ ,  $\tilde{f}^C$ , and  $\tilde{f}^{LC}$ , and encourage their interaction through another step of 3D sparse convolutions

<sup>2</sup>The neighborhood of a point is defined as a small ball with the radius of the smallest voxel's (0.075m, 0.075m, 0.2m) diagonal length, which is 0.23m. Points of such close proximity are equally treated in the following process due to the voxelization operation.

as:

$$F^M = \Phi([\tilde{f}^L, \tilde{f}^C, \tilde{f}^{LC}]; k^M), \quad (2)$$

where  $k^M$  is the kernel and  $F^M$  represents the multi-modal interacted voxel features of this stage, which will be used for a progressive fusion across multiple scales (more details in the next subsection). Since we currently focus on describing the interaction within each scale, the subscripts denoting scale are omitted.

**Multi-Scale Progressive Interaction** With the previously introduced MDU and MS-Conv, we now describe how the progressive interaction is performed across scales. For all the scales, the multi-scale LiDAR voxel features are denoted as  $\{F_i^L\}$ , multi-scale image features are denoted as  $\{P_i\}$ , and multi-scale camera voxel features  $\{F_i^C\}$  is generated from  $\{P_i\}$  via MDU. Then for each pair of  $F_i^L$  and  $F_i^C$  in each scale, we feed them to the corresponding MS-Conv block for multi-modal interaction in the voxel space and obtain the interacted feature  $F_i^M$  through Eq.(1) and (2). To further progressively aggregate multi-granularity information from multi-scale features  $\{F_i^M\}$ , we introduce cross-scale connections as shown in Fig.2, which perform the following operation for voxel features from different scales:

$$\hat{F}_{i+1}^M = F_{i+1}^M + \text{DownSample}(\hat{F}_i^M), \quad (3)$$

where the voxel downsample operation  $\text{DownSample}(\cdot)$  is applied to align their spatial resolutions, and  $\hat{F}_{i+1}^M$  is the resulting voxel features that combine multi-scale information from the current and previous scales. With the above designs, multi-granularity LiDAR-camera features can be thoroughly interacted at multiple scales in the voxel space. The final output multi-modal voxel features can serve as a powerful representation for the subsequent modules.

### 3.4 Prediction in BEV Space

Following the workflow of prevalent voxel-based 3D object detectors (Yan, Mao, and Li 2018; Zhou and Tuzel 2018; Yin, Zhou, and Krahenbuhl 2021), we compress the height of voxel features to transform them into the BEV (bird's-eye view) space. Specifically, we first fuse the LiDAR and multi-modal BEV features with a lightweight 2D convolution block (i.e., an ASPP module (Chen et al. 2017a) for nuScenes). Then, the BEV feature containing enhanced multi-modality information is fed into a conventional BEV encoder and a detection head for the final prediction. Our proposed components can be seamlessly integrated with common 3D detection architectures and can be trained in an end-to-end manner.

## 4 Experiments

### 4.1 Experimental Setup

**Dataset and Metrics** The nuScenes (Caesar et al. 2020) dataset is a large-scale autonomous driving benchmark, where six cameras, one LiDAR, and five radars are utilized to capture multi-modal data. There are 10,000 driving scenarios in total, which are split into 700, 150, and 150 scenes

| Method                                       | Modality | Map | mAP         | NDS         | Car         | Truck       | C.V.        | Bus         | Trailer     | Barrier     | Motor.      | Bike        | Ped.        | T.C.        |
|--|----------|-----|-------------|-------------|-------------|-------------|-------------|-------------|-------------|-------------|-------------|-------------|-------------|-------------|
| FUTR (Chen et al. 2022)                      | LC       | ✗   | 64.2        | 68.0        | 86.3        | 61.5        | 26.0        | 71.9        | 42.1        | 64.4        | 73.6        | 63.3        | 82.6        | 70.1        |
| TransFusion (Bai et al. 2022)                | LC       | ✗   | 67.3        | 71.2        | 87.6        | 62.0        | 27.4        | 75.7        | 42.8        | <b>73.9</b> | 75.4        | 63.1        | 87.8        | 77.0        |
| BEVFusion (Liang et al. 2022)                | LC       | ✗   | 67.9        | 71.0        | <b>88.6</b> | <b>65.0</b> | 28.1        | 75.4        | 41.4        | 72.2        | 76.7        | 65.8        | 88.7        | 76.9        |
| BEVFusion (Liu et al. 2022)                  | LC       | ✓   | 68.5        | 71.4        | -           | --          | -           | -           | -           | -           | -           | -           | -           | -           |
| MSMDFusion-T                                 | LC       | ✗   | <b>69.1</b> | <b>71.8</b> | 88.5        | 64.0        | <b>29.2</b> | <b>76.2</b> | <b>44.7</b> | 70.4        | <b>79.1</b> | <b>68.6</b> | <b>89.7</b> | <b>80.1</b> |
| PointPillar (Lang et al. 2019)               | L        | ✗   | 40.1        | 55.0        | 76.0        | 31.0        | 11.3        | 32.1        | 36.6        | 56.4        | 34.2        | 14.0        | 64.0        | 45.6        |
| CenterPoint (Yin, Zhou, and Krahenbuhl 2021) | L        | ✗   | 60.3        | 67.3        | 85.2        | 53.5        | 20.0        | 63.6        | 56.0        | 71.1        | 59.5        | 30.7        | 84.6        | 78.4        |
| TransFusion-L (Bai et al. 2022)              | L        | ✗   | 65.5        | 70.2        | 86.2        | 56.7        | 28.2        | 66.3        | 58.8        | 78.2        | 68.3        | 44.2        | 86.1        | 82.0        |
| PointPainting (Vora et al. 2020)             | LC       | ✗   | 46.4        | 58.1        | 77.9        | 35.8        | 15.8        | 36.2        | 37.3        | 60.2        | 41.5        | 24.1        | 73.3        | 62.4        |
| 3D-CVF (Yoo et al. 2020)                     | LC       | ✗   | 52.7        | 62.3        | 83.0        | 45.0        | 15.9        | 48.8        | 49.6        | 65.9        | 51.2        | 30.4        | 74.2        | 62.9        |
| PointAugmenting (Wang et al. 2021)           | LC       | ✗   | 66.8        | 71.0        | 87.5        | 57.3        | 28.0        | 65.2        | 60.7        | 72.6        | <b>74.3</b> | 50.9        | 87.9        | 83.6        |
| MVP (Yin, Zhou, and Krähenbühl 2021)         | LC       | ✗   | 66.4        | 70.5        | 86.8        | 58.5        | 26.1        | 67.4        | 57.3        | 74.8        | 70.0        | 49.3        | 89.1        | 85.0        |
| TransFusion (Bai et al. 2022)                | LC       | ✗   | 68.9        | 71.7        | 87.1        | 60.0        | 33.1        | 68.3        | 60.8        | 78.1        | 73.6        | 52.9        | 88.4        | 86.7        |
| BEVFusion (Liang et al. 2022)                | LC       | ✗   | 69.2        | 71.8        | 88.1        | 60.9        | 34.4        | 69.3        | 62.1        | 78.2        | 72.2        | 52.2        | 89.2        | 85.2        |
| BEVFusion (Liu et al. 2022)                  | LC       | ✓   | 70.2        | 72.9        | <b>88.6</b> | 60.1        | <b>39.3</b> | 69.8        | 63.8        | <b>80.0</b> | 74.1        | 51.0        | 89.2        | 86.5        |
| MSMDFusion-T (Ours)                          | LC       | ✗   | <b>70.8</b> | <b>73.2</b> | 87.9        | <b>61.6</b> | <b>38.1</b> | <b>70.0</b> | <b>64.4</b> | 79.0        | 73.9        | <b>56.6</b> | <b>89.7</b> | <b>87.1</b> |

Table 1: Comparison with state-of-the-art methods on nuScenes val (top) and test (bottom) set. MSMDFusion-T indicates that the detection head is the TransFusion Head. “Map” means whether the model introduces additional BEV map segmentation supervision for enhancement. We highlight the best performances across all methods with **bold**. Meanwhile, the best performances achieved without map data are highlighted with underline for fair comparison.

for training, validation, and testing, respectively. For 3D object detection, nuScenes defines a set of evaluation protocols, including the nuScenes Detection Score (NDS), mean Average Precision (mAP), as well as five True Positive (TP) metrics, namely mean Average Translation Error (mATE), mean Average Scale Error (mASE), mean Average Orientation Error (mAOE), mean Average Velocity Error (mAVE) and mean Average Attribute Error (mAAE). We report mAP, which is the mean of the average precision across ten classes under distance thresholds of 0.5m, 1m, 2m, 4m. NDS is the weighted combination of mAP, mATE, mASE, mAOE, mAVE and mAAE.

**Implementation Details** We use ResNet-50 (He et al. 2016) with FPN (Lin et al. 2017) as the image backbone and Vox- elNet (Yan, Mao, and Li 2018) as the LiDAR backbone. We set the image size to  $448 \times 800$ , and voxel size as  $(0.075m, 0.075m, 0.2m)$  following (Bai et al. 2022). To make the best use of multi-scale semantics, we extract features from four levels of the FPN (P2 to P5). Following MVP (Yin, Zhou, and Krähenbühl 2021), we select 50 seeds on each instance unless otherwise specified. Our model training has two stages: (1) We first train a LiDAR-only detector for 20 epochs as our 3D backbone. (2) We then connect the proposed LiDAR-camera fusion modules with the 3D backbone for a joint training of another 6 epochs. The data augmentation strategies and training schedules are the same as prior works (Yin, Zhou, and Krahenbuhl 2021; Zhu et al. 2019). We do not use Test-Time Augmentation (TTA) or multi- model ensemble during inference.

## 4.2 Comparison with State-of-the-art

We compare our MSMDFusion with state-of-the-art approaches on the nuScenes validation set and test set. Overall, we can observe from Table 1 that our method surpasses all existing methods, and achieves the new state-of-

the-art performances on both nuScenes validation set (69.1% mAP and 71.8% NDS) and test set (70.8% mAP and 73.2% NDS). Specifically, for fair comparison, we also compare our method with all approaches that *do not use additional map data* for supervision. The results show that our MSMDFusion achieves 1.6% mAP and 1.4% NDS improvements on the nuScenes test set than the strongest competitor, BEVFusion (Liang et al. 2022). Meanwhile, our method maintains consistent performance advantages on most object categories, especially on the challenging categories: *C.V.* and *Bike*, where a 3.7% absolute AP gains over the strongest competitors are achieved for both. Then we compare our method with the strong BEVFusion (Liu et al. 2022) that utilizes additional BEV map segmentation supervision by performing multi-task learning. By comparing the last two rows of Table 1, it can be seen that although without map data supervision, our method still outperforms it in most cases, which proves the superiority of our MSMDFusion.

Since our MSMDFusion and two BEVFusion methods all fuse LiDAR and camera signals via generating 3D virtual points from 2D seeds, we specifically compare our method with them in terms of the number of generated virtual points per LiDAR frame as shown in Table 2. The results suggest that although with 100 times fewer generated virtual points (16k vs 2M/5M) than them, our MSMDFusion still outperforms them in both mAP and NDS, which proves the superiority of our multi-depth virtual points generation strategy and multi-scale multi-modal fusion framework.

Besides, to investigate our method’s generalization ability on other datasets and other architectures of detectors, we also perform extensive experiments on the **KITTI** dataset with the **MSMDFusion-C** (i.e., the CenterPoint version of our method). Meanwhile, we also provide abundant qualitative results of the generated virtual points and 3D object detections. Above results are placed in the supplementary

| Method                        | NVPF <sup>3</sup> | mAP         | NDS         |
|-------------------------------|-------------------|-------------|-------------|
| BEVFusion (Liang et al. 2022) | 5M                | 69.2        | 71.8        |
| BEVFusion (Liu et al. 2022)   | 2M                | 70.2        | 72.9        |
| MSMDFusion-T(Ours)            | 16k               | <b>70.8</b> | <b>73.2</b> |

Table 2: Number of Virtual points Per Frame (NVPF) and performance comparison with two strongest methods on nuScenes test set.

materials due to page limit.

### 4.3 Comprehensive Analysis

**Ablation of proposed components** We conduct comprehensive ablation studies for each of our proposed components as shown in Table 3. We use TransFusion-L (Bai et al. 2022) as our baseline (#1), and use the image feature P3 when only performing single-scale fusion. Besides, for experiments that perform multi-scale interaction without MS-Conv, we substitute MS-Conv with a 3D sparse convolution block whose number of parameters are similar to MS-Conv, and the mixed LiDAR and camera voxel features are directly fed into this convolution block.

From the results of the Table 3, we have the following observations. (i) Introducing virtual points for multi-modal interaction (#2, #3, and #4) brings evident improvements over the baseline, which proves that fusing dense 2D semantics from virtual points with LiDAR features in the voxel space can significantly enhance the LiDAR-only detector. (ii) Sampling seeds from both instance boundary and inner region (#4) can lead to better performances than from only one of the two regions (#2 and #3). This combined sampling strategy can more comprehensively capture objects’ characteristics. And using the proposed Multi-Depth Unprojection strategy can bring a further improvement of 0.27% mAP (#5). (iii) Multi-scale LiDAR-camera fusion (#6) has a significant advantage (+0.44% mAP) over single-scale fusion (#4), and our proposed MS-Conv is a strong enhancement (#7) that continues to improve the multi-scale fusion model by another 0.2% mAP and 0.4% NDS, while the number of parameters are not increased. (iv) With all these components combined (#8), the final mAP and NDS are significantly increased from 64.56% to 69.09% and 69.69% to 71.77%, respectively, which proves the effectiveness of our designs.

**Effects of the number of depths in MDU** To further inspect the effects of the Number of Depths Per Seed (NDPS) in MDU, we keep other settings unchanged and vary NDPS to compare the performances. As Table 4 shows, increasing NDPS from 1 to 6 can gradually improve these models’ performances. As we previously analyzed in Fig.4, such improvements can be mainly attributed to the increased recall and tolerable distance error of the virtual points. However, when NDPS increases to 10, the model’s performance drops because the extra noise diminishes the benefits of correctly

<sup>3</sup>NVPF of BEVFusion (Liang et al. 2022) is calculated with its official code. BEVFusion (Liu et al. 2022) reports its NVPF in the paper. The former has a higher NVPF because it generates virtual points from image features of larger resolution.

| # | boundary | inner | multi-depth | multi-scale | MS-C | mAP   | NDS   |
|---|----------|-------|-------------|-------------|------|-------|-------|
| 1 |          |       |             |             |      | 64.56 | 69.69 |
| 2 | ✓        |       |             |             |      | 67.09 | 70.64 |
| 3 |          | ✓     |             |             |      | 67.23 | 70.67 |
| 4 | ✓        | ✓     |             |             |      | 67.85 | 71.04 |
| 5 | ✓        | ✓     | ✓           | ✓           |      | 68.12 | 71.12 |
| 6 | ✓        | ✓     |             |             | ✓    | 68.29 | 71.02 |
| 7 | ✓        | ✓     |             | ✓           | ✓    | 68.49 | 71.42 |
| 8 | ✓        | ✓     | ✓           | ✓           | ✓    | 69.06 | 71.77 |

Table 3: Ablation studies for our proposed components on the nuScenes validation set. “MS-C” represents MS-Conv, and “multi-scale” means performing multi-scale fusion without MS-Conv.

| NDPS | NSPI | mAP          | NDS          |
|------|------|--------------|--------------|
| 1    | 50   | 68.49        | 71.42        |
| 3    | 50   | 68.72        | 71.58        |
| 6    | 50   | <b>69.06</b> | <b>71.77</b> |
| 10   | 50   | 68.78        | 71.58        |
| 1    | 200  | 68.18        | 71.02        |

Table 4: Effects of the Number of Depths Per Seed (NDPS) and Number of Seeds Per Instance (NSPI) in Multi-Depth Unprojection.

generated virtual points. Moreover, we also study whether increasing the number of seeds per instance (NSPI) can achieve similar improvements, and the results with 1 NDPS and 200 NSPI are shown in the last row of Table 4. It can be seen that simply increasing seeds cannot bring improvements as our multi-depth strategy, but can even hurt performance due to more noise from single-depth unprojection.

**Effects of multi-scale interaction** We also investigate the effects of performing LiDAR-camera interaction at different scales. As shown in Table 5, for models with single-scale interaction (#2-#4), interacting at scales of larger spatial resolution generally leads to larger performance gains over the baseline (#1), which mainly benefits from more fine-grained image and LiDAR features. If the multi-modal interaction is performed at more scales (#6-#8), multi-granularity information can be integrated into our progressive interaction process to consistently achieve better performances than single-scale models. The complete multi-scale interaction model achieves performance gains of  $\sim 1\%$  mAP and 0.65 NDS over the best single-scale model, which indicates that multi-scale interaction is beneficial for comprehensive multi-modal fusion.

**Effects of model size** We vary the number of parameters of our multi-modal interaction components (MS-Conv) and test their performances to verify that the improvements are not simply because of the increased model capacity. Table 6 shows the performances of three models of different sizes. Specifically, compared to our final model (“medium”), the “small” model with about half of its parameters can achieve similar performances. And further increasing the model capacity to “large” does not bring extra improvements. This

| # | P2 | P3 | P4 | P5 | mAP          | NDS          |
|---|----|----|----|----|--------------|--------------|
| 1 |    |    |    |    | 64.56        | 69.69        |
| 2 | ✓  |    |    |    | 68.09        | 71.19        |
| 3 |    | ✓  |    |    | 68.12        | 71.12        |
| 4 |    |    | ✓  |    | 67.71        | 70.93        |
| 5 |    |    |    | ✓  | 67.29        | 70.77        |
| 6 | ✓  | ✓  |    |    | 68.57        | 71.44        |
| 7 | ✓  | ✓  | ✓  |    | 68.85        | 71.46        |
| 8 | ✓  | ✓  | ✓  | ✓  | <b>69.06</b> | <b>71.77</b> |

Table 5: Effects of LiDAR-camera interaction at different scales, P2-P5 represent the scales where the spatial resolutions of the features decrease from P2 to P5.

| Size   | Params | mAP          | NDS          |
|--------|--------|--------------|--------------|
| small  | 53M    | 68.97        | <b>71.81</b> |
| medium | 93M    | <b>69.06</b> | 71.77        |
| large  | 154M   | 68.98        | 71.78        |

Table 6: Effects of using different numbers of parameters for multi-modal interaction (MS-Conv). “medium” is our final model.

demonstrates that parameter size hardly affects our model’s performance, and our multi-scale LiDAR-camera interaction and multi-depth unprojection strategy are indeed the main contributing factors.

## 5 Conclusion

In this paper, we present MSMDFusion, a novel LiDAR-camera fusion framework for 3D object detection which performs multi-modal interaction across multiple scales. We adopt a Multi-Depth Unprojection (MDU) strategy to obtain reliable virtual points from images, and apply Modality-Specific Convolution (MS-Conv) in each scale to encourage fine-grained multi-modal fusion. Multi-granularity information is further combined across scales to form comprehensive features for the prediction head. Extensive experiments demonstrate the effectiveness of these components and our method finally achieves state-of-the-art performances on the nuScenes dataset.

## References

- Bai, X.; Hu, Z.; Zhu, X.; Huang, Q.; Chen, Y.; Fu, H.; and Tai, C.-L. 2022. Transfusion: Robust lidar-camera fusion for 3d object detection with transformers. In *Proceedings of the IEEE/CVF Conference on Computer Vision and Pattern Recognition*, 1090–1099.
- Caesar, H.; Bankiti, V.; Lang, A. H.; Vora, S.; Liang, V. E.; Xu, Q.; Krishnan, A.; Pan, Y.; Baldan, G.; and Beijbom, O. 2020. nuScenes: A multimodal dataset for autonomous driving. In *CVPR*.
- Chen, L.-C.; Papandreou, G.; Schroff, F.; and Adam, H. 2017a. Rethinking atrous convolution for semantic image segmentation. *arXiv preprint arXiv:1706.05587*.
- Chen, X.; Ma, H.; Wan, J.; Li, B.; and Xia, T. 2017b. Multi-view 3d object detection network for autonomous driving. In *Proceedings of the IEEE conference on Computer Vision and Pattern Recognition*, 1907–1915.
- Chen, X.; Zhang, T.; Wang, Y.; Wang, Y.; and Zhao, H. 2022. Futr3d: A unified sensor fusion framework for 3d detection. *arXiv preprint arXiv:2203.10642*.
- Graham, B.; Engelcke, M.; and Van Der Maaten, L. 2018. 3d semantic segmentation with submanifold sparse convolutional networks. In *Proceedings of the IEEE conference on computer vision and pattern recognition*, 9224–9232.
- He, K.; Zhang, X.; Ren, S.; and Sun, J. 2016. Deep residual learning for image recognition. In *Proceedings of the IEEE conference on computer vision and pattern recognition*, 770–778.
- Huang, J.; Huang, G.; Zhu, Z.; and Du, D. 2021. Bevdet: High-performance multi-camera 3d object detection in bird-eye-view. *arXiv preprint arXiv:2112.11790*.
- Huang, T.; Liu, Z.; Chen, X.; and Bai, X. 2020. Epnet: Enhancing point features with image semantics for 3d object detection. In *European Conference on Computer Vision*, 35–52. Springer.
- Ku, J.; Mozifian, M.; Lee, J.; Harakeh, A.; and Waslander, S. L. 2018. Joint 3d proposal generation and object detection from view aggregation. In *2018 IEEE/RSJ International Conference on Intelligent Robots and Systems (IROS)*, 1–8. IEEE.
- Lang, A. H.; Vora, S.; Caesar, H.; Zhou, L.; Yang, J.; and Beijbom, O. 2019. Pointpillars: Fast encoders for object detection from point clouds. In *Proceedings of the IEEE/CVF conference on computer vision and pattern recognition*, 12697–12705.
- Li, Y.; Ge, Z.; Yu, G.; Yang, J.; Wang, Z.; Shi, Y.; Sun, J.; and Li, Z. 2022. BEVDepth: Acquisition of Reliable Depth for Multi-view 3D Object Detection. *arXiv preprint arXiv:2206.10092*.
- Liang, M.; Yang, B.; Chen, Y.; Hu, R.; and Urtasun, R. 2019. Multi-task multi-sensor fusion for 3d object detection. In *Proceedings of the IEEE/CVF Conference on Computer Vision and Pattern Recognition*, 7345–7353.
- Liang, M.; Yang, B.; Wang, S.; and Urtasun, R. 2018. Deep continuous fusion for multi-sensor 3d object detection. In *Proceedings of the European conference on computer vision (ECCV)*, 641–656.

- Liang, T.; Xie, H.; Yu, K.; Xia, Z.; Lin, Z.; Wang, Y.; Tang, T.; Wang, B.; and Tang, Z. 2022. BEVFusion: A Simple and Robust LiDAR-Camera Fusion Framework. *arXiv preprint arXiv:2205.13790*.
- Lin, T.-Y.; Dollár, P.; Girshick, R.; He, K.; Hariharan, B.; and Belongie, S. 2017. Feature pyramid networks for object detection. In *Proceedings of the IEEE conference on computer vision and pattern recognition*, 2117–2125.
- Liu, Z.; Tang, H.; Amini, A.; Yang, X.; Mao, H.; Rus, D.; and Han, S. 2022. BEVFusion: Multi-Task Multi-Sensor Fusion with Unified Bird’s-Eye View Representation. *arXiv preprint arXiv:2205.13542*.
- Philion, J.; and Fidler, S. 2020. Lift, splat, shoot: Encoding images from arbitrary camera rigs by implicitly unprojecting to 3d. In *European Conference on Computer Vision*, 194–210. Springer.
- Qi, C. R.; Liu, W.; Wu, C.; Su, H.; and Guibas, L. J. 2018. Frustum pointnets for 3d object detection from rgbd data. In *Proceedings of the IEEE conference on computer vision and pattern recognition*, 918–927.
- Sindagi, V. A.; Zhou, Y.; and Tuzel, O. 2019. Mvx-net: Multimodal voxelnet for 3d object detection. In *2019 International Conference on Robotics and Automation (ICRA)*, 7276–7282. IEEE.
- Vora, S.; Lang, A. H.; Helou, B.; and Beijbom, O. 2020. Pointpainting: Sequential fusion for 3d object detection. In *Proceedings of the IEEE/CVF conference on computer vision and pattern recognition*, 4604–4612.
- Wang, C.; Ma, C.; Zhu, M.; and Yang, X. 2021. Pointaugmenting: Cross-modal augmentation for 3d object detection. In *Proceedings of the IEEE/CVF Conference on Computer Vision and Pattern Recognition*, 11794–11803.
- Wang, Y.; Chao, W.-L.; Garg, D.; Hariharan, B.; Campbell, M.; and Weinberger, K. Q. 2019. Pseudo-lidar from visual depth estimation: Bridging the gap in 3d object detection for autonomous driving. In *Proceedings of the IEEE/CVF Conference on Computer Vision and Pattern Recognition*, 8445–8453.
- Yan, Y.; Mao, Y.; and Li, B. 2018. Second: Sparsely embedded convolutional detection. *Sensors*, 18(10): 3337.
- Yin, T.; Zhou, X.; and Krahenbuhl, P. 2021. Center-based 3d object detection and tracking. In *Proceedings of the IEEE/CVF conference on computer vision and pattern recognition*, 11784–11793.
- Yin, T.; Zhou, X.; and Krähenbühl, P. 2021. Multimodal virtual point 3d detection. *Advances in Neural Information Processing Systems*, 34: 16494–16507.
- Yoo, J. H.; Kim, Y.; Kim, J.; and Choi, J. W. 2020. 3d-cvf: Generating joint camera and lidar features using cross-view spatial feature fusion for 3d object detection. In *European Conference on Computer Vision*, 720–736. Springer.
- Zhou, Y.; and Tuzel, O. 2018. Voxelnet: End-to-end learning for point cloud based 3d object detection. In *Proceedings of the IEEE conference on computer vision and pattern recognition*, 4490–4499.
- Zhu, B.; Jiang, Z.; Zhou, X.; Li, Z.; and Yu, G. 2019. Class-balanced grouping and sampling for point cloud 3d object detection. *arXiv preprint arXiv:1908.09492*.